Markó *et al. Geothermal Energy* (2024) 12:40
https://doi.org/10.1186/s40517-024-00317-2

Geothermal Energy

RESEARCH Open Access

Controls of low injectivity caused by interaction of reservoir and clogging processes in a sedimentary geothermal aquifer (Mezőberény, Hungary)

Ábel Markó[1*], Maren Brehme[2,3], Daniele Pedretti[4], Günter Zimmermann[3] and Ernst Huenges[3]

*Correspondence:
marab@student.elte.hu

[1] ELTE Eötvös Loránd University, Institute of Geography and Earth Sciences, Department of Geology, Pázmány P. Stny. 1/c, 1117 Budapest, Hungary
[2] Department of Earth Sciences, ETH Zürich, Geothermal Energy and Geofluids, Sonneggstrasse 5, 8092 Zurich, Switzerland
[3] Section Geoenergy, Helmholtzh Centre Potsdam, GFZ German Research Center for Geosciences, Telegrafenberg, 14473 Potsdam, Germany
[4] Dipartimento di Scienze della Terra "A. Desio", Università degli Studi di Milano (UNIMI), Via Mangiagalli 34, 20133 Milan, Italy

Abstract

Low injectivity is often experienced in geothermal doublets installed in sandstone reservoirs. This even led to a shutdown of the Mezőberény (Hungary) geothermal site. An on-site campaign was carried out in January 2021 to prepare a stimulation aiming to enhance the transmissivity of the sedimentary reservoir and the near-wellbore zone of this site. Previous studies have concluded that insufficient injectivity may be linked to a high skin effect in the near well-bore zone and pore clogging in combination with the low net sandstone content of the fluvio-deltaic reservoir. A chemical soft stimulation based on the injection of hydrochloric acid (HCl) was successfully used to unclog and recover the well injectivity. Despite such empirical evidence, the geochemical mechanisms leading to both, detrimental formation of clogging and the HCl-driven transmissivity restoration, have not yet been elucidated. This work presents the results of a novel analysis aiming at (a) predicting the dominant type of clogging forming in the near-well bore zone; (b) quantifying the drop in hydraulic conductivity as clogging occurs; and (c) supporting the optimization of the HCl dosage during the chemical soft stimulation. The study is supported by new experimental datasets never presented before from the Mezőberény site and a geochemical model set-up simulating the main mechanisms involved in the clogging and unclogging processes. It is concluded that the biofilm formation was the dominant, while the precipitation of calcite and amorphous ferrihydrite—later reduced to magnetite by microbes—was the secondary clogging mechanism: In the long-term (yearly scale) simulating the hydraulic conductivity showed a decline with forming scales; therefore, biofilm was presumably responsible for the experienced rapid (1 month) clogging. When modelling the chemical stimulation, the estimated amount of precipitated minerals was dissolved already with 2.5 mol of HCl per liter of water (~ 10 m/m%). Therefore, the 20 m/m% of HCl chosen during the field campaign might had a beneficial effect dissolving the potentially higher amount of scaling and/or the carbonate minerals of the matrix near the wellbore. Overall, it is concluded that the chemical and the microbial analyses together with the geochemical model were critical to tailor the remediation attempts and to propose further development or reconstruction of the surface system before going into operation to prevent recurrent impairments.

Our findings highlight the importance of interactions of various clogging mechanisms with each other as well as with the reservoir processes and provide approaches to tackle the issue of injectivity drop by characterizing and quantifying their effects.

Keywords: Geothermal reinjection, Clogging, Sandstone aquifer, Thermal water, Geochemical modelling, Injectivity enhancement, Soft stimulation

Introduction

Injection issues frequently arise at geothermal reinjection sites in siliciclastic aquifers while they are in use (Ungemach 2003; Kamila et al. 2020; Song et al. 2020; Luo et al. 2023). The low injectivity hinders sustainable thermal water utilization that requires the support of natural replenishment through reinjection (Gringarten 1978; Stefansson 1997; Axelsson 2012). Low injectivity can originate from various factors, among others the initial geological-hydrogeological conditions and the disturbed physico-chemical equilibrium changed by drilling and by production and injection (Szanyi et al. 2014; Markó et al. 2021). This triggers physical, chemical and biological clogging processes which can lead to damage to the well, the near-wellbore zone and the formation (Brehme et al. 2018; Brehme et al. 2019a). For example, the exsolution of CO_2 triggers calcite precipitation (Cosmo et al. 2022), while mixing induced redox reactions can lead to bioclogging (Burté et al. 2019) which is favoured by the high amount of dissolved organic compounds (Osvald et al. 2017; Leins et al. 2022).

Revealing the interaction of the reservoir and local clogging processes is essential for reaching progress in understanding and preventing injectivity decline in sandstone aquifers. Clogging products reduce the porosity and permeability in the reservoir, thus increasing pump energy losses.

Hydrogeochemical models have been widely adopted for the prediction of clogging in multiple contexts (Brehme et al. 2018; Yanaze et al. 2019; Kazmierczak et al. 2022). However, these models typically require a large number of input data, which encompass mineralogical, chemical and microbiological properties of the native reservoir and the native and injected waters. This may explain why the use of (hydro)geochemical models remains limited in the context of well clogging analysis (Hörbrand et al. 2018; Alsemgeest et al. 2021; Zacherl and Baumann 2023).

The Mezőberény geothermal site is an example site that suffers from low injectivity because of pore clogging and low reservoir performance. Since 2021, several studies have been conducted on the site (a brief review is provided in section "Site description and background knowledge"). Recently, Brehme et al. (2024) presented the approach and the results of a chemical soft stimulation based on the injection of HCl, which successfully led to unclog the system and enhanced the well injectivity. Despite the empirical evidence, the geochemical mechanisms that can lead to the formation and subsequent removal of clogging by HCl injection have not been quantified. A geochemical model that could help quantifying the amount of clogging and the change in hydraulic conductivity has not been developed yet. Such a model could assist decision makers in accurately designing and optimizing the chemical soft stimulation as well as other operations on the site.

The purpose of this work was to fill up these gaps, in two ways. First, we present new and until now unpublished results of the site, which include detailed chemical,

mineralogical and microbial analyses of the samples taken from the well bore along with logging and well test results. Such data are examined in depth to gain a conceptual understanding of the most likely clogging processes that could form in the near-wellbore zone. Second, we present an analysis based on a new geochemical model set-up that can quantify (a) the mass of clogging materials; (b) their volumetric impact on the total porosity and its effect on the reduction of the hydraulic conductivity; and (c) the impact of HCl addition on precipitated minerals (i.e., their dissolution resulting in the restoration of the permeability. The overarching goal is to show that a combination of detailed experimental studies and geochemical modelling can provide key insight into the understanding of geochemical and reservoir scale processes in sedimentary basements, helping to avoid injection related problems and optimize the well injectivity.

Methods and data

Site description and background knowledge

The Mezőberény site is located in the Békés Basin, southeastern Hungary (Fig. 1). As part of the Pannonian Basin, the area is characterized by excellent geothermal potential represented by the average geothermal gradient of 45 °C/km (Dövényi and Horváth 1988; Grow et al. 1994). During the Miocene-Pliocene the basin as well as the Lake Pannon was filled with thousands of meters of siliciclastic sediments. Within this geological framework, the shallow-water Pannonian Formations, deposited in deltaplain, deltafront (Újfalu Formation) and alluvial (Zagyva Formation) environments serve as pivotal thermal water aquifers (Sztanó et al. 2013; Horváth et al. 2015), belonging to the Great Plain Aquifer (Tóth and Almási 2001). Although their exploitation has almost one century long history, reinjection of heat-depleted water operates at only a small portion of the sites (Szanyi and Kovács 2010; Békési et al. 2022). Recent findings further highlight the importance of reinjection as plenty of the thermal water wells target the newly identified, so-called transition zone of the Great Plain Aquifer, which is characterized by limited or no natural replenishment from the surface and the topography driven zone

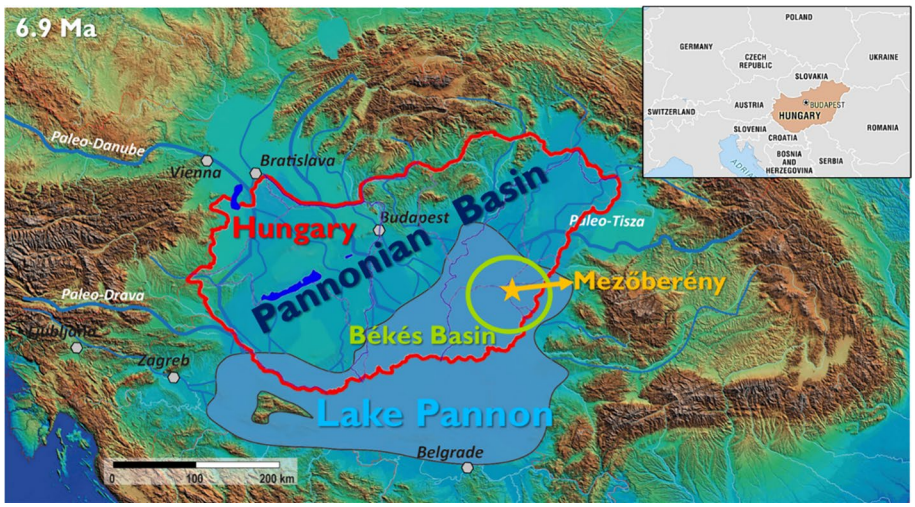

Fig. 1 Location of the Mezőberény study site within the Pannonian Basin and with the extent of the Lake Pannon 6.9 million years ago [modified from Sztanó et al. (2020)]

(Czauner et al. 2024). Accordingly, the need for artificial replenishment through reinjection is crucial.

Like dozens of geothermal sites in SW Hungary, the Mezőberény doublet aimed to exploit thermal water from the permeable sandstone bodies of the Pannonian aquifers. Permeability of the latter bodies can reach 500–1500 mD with a bulk porosity of 20 to 30% (Tóth & Almási 2001; Bobok & Tóth 2003; Koroncz et al. 2022). Recent studies revealed sandstone permeabilities below previously published averages ranging from several tens of mD to 400 mD due to the heterogenous characteristic of the aquifer (Willems et al. 2021; Njeru et al. 2024). Statistical evaluation of historical micromineralogical analyses—performed macroscopically, and using binocular stereo—and petrographic microscope on drilling samples from Újfalu and Zagyva Formation (from the Dunántúl Group) showed the presence of quartz (SiO_2), K-feldspar ($KAlSi_3O_8$), chlorite (14A) ($Mg_5Al_2Si_3O_{10}(OH)_8$, K-mica ($KAl_3Si_3O_{10}(OH)_2$), pyrite (FeS_2), goethite (FeO(OH)) (Juhász & Thamó-Bozsó, 2006; Thamó-Bozsó et al. 2006). XRD and XRF analysis on samples from similar depth detected quartz, muscovite ($KAl_3Si_3O_{10}(OH)_2$), dolomite $CaMg(CO_3)_2$, albite ($NaAlSi_3O_8$), chlorite, calcite (GeoCom 2013; Koroncz et al. 2022). The mainly poor cementation is formed by carbonates (calcite, dolomite) and clay minerals (sericite, montmorillonite, kaolinite, and illite) (Koroncz et al. 2022).

The Mezőberény geothermal site (SE Hungary) was constructed between 2011 and 2012. The two wells forming the doublet are cased and screened with Johnson filters and gravel pack starting from 1600 to 2000 m depth (Fig. 2). Screened intervals filter the sandy bodies of the shallow-water Pannonian aquifer (Fig. 2A, B). Thermal fluid is extracted using a submersible pump and directed to a buffer tank (50 m^3), which also serves as a degassing tank. After degassing, booster pumps propel the water through quartz-sand filters, and its heat is transferred to heat consumers. The heat-depleted water returns to another buffer tank and passes through filters before being reinjected into the reservoir (Markó et al. 2021). The injection well structure contains all together 12 screened sections with a cumulative length of 75.5 m (Fig. 2B). According to the flow tests performed after installation in 2012, out of the total length, 43.3 m was considered as operating interval (VITUKI 2012; Markó et al. 2021).

The initial hydraulic parameters of the injector are as follows: the permeability of the screened sections derived from pressure buildup tests is 8.79×10^{-14} m^2, with the corresponding transmissivity of 1.26×10^4 m^2/s, while the productivity was 1707 m^3/day/MPa (VITUKI 2012; Markó et al. 2021). These parameters were found to be relatively low compared to similar sites in the region (Markó et al. 2021).

The chemical composition of the water analyzed after the well completion shows $NaHCO_3$ type water with total dissolved solids of 6705 mg/L (production well) and 4744 mg/L (injection well) (Table 1): ion balance error was < 2%). There is a significant gas content, with 59%v/v and 81.66%v/v methane in the production well and injection well, respectively (Table 2).

History and potential causes of low injectivity

A strong drop in injectivity was experienced within one month after starting the operation in 2012–2013: the original maximum injection rate of 400 L/min dropped

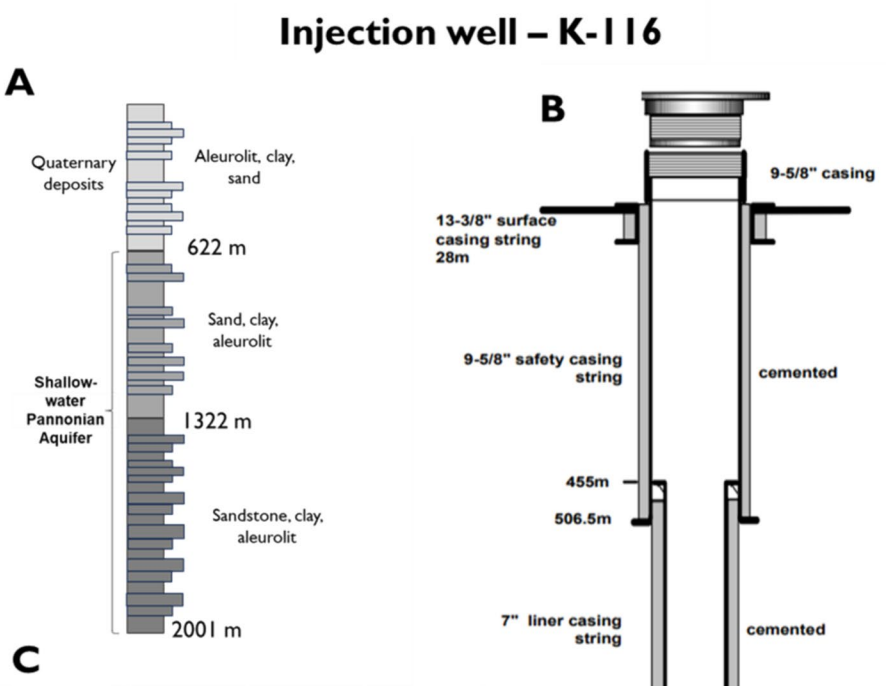

C

Number	Top (m)	Bottom (m)	Length (m)
I.	1643.5	1646.8	3.3
II.	1657.9	1661.6	3.7
III.	1664.6	1669.2	4.6
IV.	1743.6	1754.5	10.9
V.	1791.6	1794.5	2.9
VI.	1809.6	1818.5	8.9
VII.	1854.6	1860.5	5.9
VIII.	1864	1870	6
IX.	1880.5	1886.5	6
X.	1889.6	1895.4	5.8
XI.	1896.6	1902.5	5.9
XII	1918.8	1930.4	11.6
	All screens		75.5

Fig. 2 Structure of the injection well: **A** Stratigraphy; **B** Well structure; **C** Parameters of the installed well screens of the injector

to a maximum of 40–50 L/min injection rate. During the remediation attempt in 2016–2017, cleaning of the well was carried out and clogging material was extracted; however, the system was not restarted due to lack of understanding of the reasons for low injectivity (Brehme et al. 2019b; Markó et al. 2021). Following several ideas and unsuccessful attempts to remediate and restart the operation, in 2018 the site joined the Horizon2020 DESTRESS project. The project aimed to provide solutions to enhance the production and injection of geothermal systems using soft stimulation (thermal, hydraulic and chemical) treatments (Huenges et al. 2021).

Preliminary studies by Brehme et al. (2019b, 2021) and Markó et al. (2021) concluded that the fundamental reason behind the low injectivity of this well site could be ascribed to the insufficient transmissivity of the native geological reservoir. Through

Table 1 Chemical analysis of the fluids measured after the installation of the production well (Mezőberény B-115) and the injection well (Mezőberény K-116)

Sample	Units	MEZŐBERÉNY	
		B-115	K-116
Well type		Production	Injection
Location of sampling		Surface	Surface
Flow rate during sampling	L/min	310	285
Sample date		2011 September	2012 June
pH	–	7.5	7.6
Electrical conductivity (20 °C)	[µS/cm]	5600	5360
Total dissolved solids—TDS	[mg/L]	6705	4743.86
T	[°C]	76.9	75
HCO_3^-	mg/L	4470	4570
F^-		1.7	1.56
Cl^-		268	148
Br^-		2.2	2.6
I^-		2.9	2.6
NO_3^-		< 1	< 0.02
SO_4^{2-}		20	19
Na^+		1860	1770
K^+		30	28
Ca^{2+}		13.7	17.2
Mg^{2+}		3.7	5.9
Fe		7.5	4.8
Mn		0.1	0.09
Li^+		0.55	0.49
Ba^{2+}		1.99	1.99
SiO_2		79	79
NH_4^+		24.4	28
PO_4^{3-}		0.24	0.1

Table 2 Separated gas compositions measured after the installation, sampled from the production well (Mezőberény B-115) and the injection well (Mezőberény K-116)

	Mezőberény (%)	
	Production well	Injection well
	B-115	K-116
O_2	0.73	0.72
CO_2	37.71	14.29
N_2	2.63	3.3
CH_4	58.93	81.66

historical data processing with analysis of the system and the wells, it was postulated that the low sandstone content of the porous reservoir could result in a limited reservoir volume and low pore connectivity (Willems et al. 2019; Markó et al. 2021; Budai et al. 2024). Additionally, it was hypothesized that the effective aquifer transmissivity was limited by the blocked pore throats and skin around the wellbore induced by microbial and chemical clogging processes. Microbial clogging (or bioclogging) is

favoured by high organic content (BTEX, phenol, and PAH) in the fluid composition, and formed by sulphate reducing and phenol degrading microbes (Brehme et al. 2021; Markó et al. 2021). As part of the workflow, potential problems due to unfavourable regional hydraulic conditions were also analysed. In the Pannonian Basin, an elevated hydraulic head has been experienced due to the connection with the underlying overpressured regime (Tóth and Almási 2001; Czauner and Mádl-Szőnyi 2011, 2013; Mádl-Szőnyi and Simon 2016). However, this elevated hydraulic head was not detectable in the close surroundings of Mezőberény. Accordingly, hydraulic conditions are favourable for low pressure reinjection, therefore their contribution to the low well efficiency is unlikely (Markó et al. 2021).

On-site investigation

Mineralogical, chemical, microbial properties of the bailer-collected sample

A sample of well bottom sediments was collected using a bailer during the cleaning of the well and the slickline sampling to obtain information about the material presumably filling the well and the well screens. The material was then analysed using X-ray Fluorescence analysis to examine its chemical composition and X-ray powder diffraction analysis to examine its mineral composition at the Laboratory of University of Miskolc. Practically used detections limits (m/m%) were: 0.01 for SiO_2, Al_2O_3; and 0.01 for MgO, CaO, Nal_2O_3, K_2O, Fe_2O_3 and 0.005 for Fe_2O_3, P_2O_5, S, MnO, TiO_2. Further optical parameters were investigated through stereo microscopy, polarizing microscopy, and Scanning Electron Microscopy Energy Dispersive Spectrometer. Two grams of the sample were washed in acetone to release the fines to obtain the coarse-grained fraction. Magnetic fraction from the latter was separated with a strong magnet from the rest of the sample. Using another part of the bailer-collected sample, DNA sequencing (PCR, capillary sequencing, and Fastq sequencing) was carried out at the laboratory of the Biological Research Centre Szeged to reveal the microbial composition of the sample.

Evaluation of the well status and the reservoir

The current state of the well and the near-wellbore reservoir had to be newly characterized, since the last intervention ended in 2017 and the last sources of information were six years old. Furthermore, additional measurements were required to complement the existing dataset. As a prerequisite, well integrity was determined by evaluating the casing, cement quality, sand screens and gravel pack positioning and state. Consequently, the well logging program covered logging for evaluating the integrity and condition of the well using Caliper, Casing Collar Locator (CCL), Radial Bond Logging (RBL), Gamma-Gamma Gravel. Additional wireline logs were acquired including dual space neutron (NTS + NTL) and Natural Gamma Ray. Near and far neutron counts were used to qualitatively account for density variations, while Gamma Ray could be used to investigate the location of the sandy intervals as well as the filters with gravel packs.

During the installation of the injection well, natural gamma and resistivity logs were used to characterize the sedimentary aquifer. Together with temperature and flow meter logs they contributed to locate the most permeable zones for placing well-screens and determine the activity of the installed screens. During the field operation in February

2021 this needed to be verified. For this purpose, natural gamma, neutron porosity and temperature logs were used.

Near and far neutron counts are used to qualitatively account for density or porosity variations. Breaking down the individual screens shows the higher and lower densities with lower and higher count rate ratios. For each screen, a Gaussian fit of the bin counts for the near to far ratio was obtained. The mean of this distribution is used as a measure of the density or porosity. To rank specific screens, it was necessary to scale the individual screens by the overall sum of the derived means (NFR/NFR) and order by the derived ratios. Neutronporosity logs contributed to decide where and how to stimulate, i.e., to choose horizons and amount of planned chemical injection volume combined with the differential temperature profile showing the activity of the screened sections.

After stating that the well integrity is suitable for further operation, a step rate injection test aimed to estimate the baseline injectivity index of the well as well as to obtain the maximum flow rate for the constant injection test. Injected fluid consisted of 4% KCl, 1.020 kg/l to prevent clay swelling, combined with citric acid, to get a pH of 5.5 and thus prevent precipitation of iron minerals triggered by the oxygen enriched injected water. During the third step, the pumping rate had to be reduced since well head pressure exceeded the previously defined maximum value of 60 bars. Step rate and constant injection tests aimed to quantify the injectivity of the well, as well as the potential skin in the near-wellbore zone. For well test analysis flow rates and downhole memory tool pressures measured at 1546 m MD were used. Absolute pressures were converted into differential pressures with the initial pressure set to zero. Using downhole pressure values and flow rates a permeability was calculated with the software package of Ecrin Saphir (Kappa Engineering) and the following input parameters using basic assumed values: porosity: 20%, well radius: 0.05715 m, pay zone (i.e., screened interval) = 75.55 m, fluid type: water viscosity: 8.5×10^{-4} Pa.

Temperature logging performed before and after the cold-water injection were used to assess the activity of the screened sections.

Geochemical modelling

A geochemical model set-up was developed to obtain quantitative information regarding the formation of well clogging. Specifically, we modelled the key processes (mixing solutions with different compositions and water–rock interaction) that lead to clogging through the precipitation of calcite ($CaCO_3$) and iron(III)hydroxides ($Fe(OH)_3$)(a). We used the widely adopted geochemical code PHREEQC v.3 (Parkhurst and Appelo 2013), which can perform a wide range of kinetic and equilibrium reactions in batch reactors or in simple dynamic flow fields. Our model set-up is based on the standard PHREEQC thermodynamic database (*phreeqc.dat*), which contains the main components, aqueous species and mineral phases required for the goals of this study. The PHREEQC model was used to calculate the Saturation Index (SI) of specific minerals and to quantify the molar amount of the precipitation, which was used for the calculation of clogged pore volumes and then the decrease in gravel pack permeability.

The geochemical setup was based on a reaction pathway (modified from Markó etal. 2020, 2021), which closely reproduces the main phases of groundwater geochemical

transformation from its production to its reinjection to the reservoir. The main steps as follows:

- Step 1 simulates the initial interaction of groundwater with the atmospheric gases. When extracted from the ground, pumped-out (i.e., produced) water (composition: Table 1) is under reducing conditions. Such water is deposited in a buffer and subsequently in a degassing tank located on the ground surface. When in contact with air and loosing dissolved gas, precipitation of iron (III) hydroxide ($Fe(OH)_3(a)$) and calcite ($CaCO_3$) is expected to occur—assuming that crystallization nuclei are present in the water—and, therefore, induced in the model, as driven by change in redox conditions.
- Step 2 simulates the effect of heat depletion from the groundwater. The water inherited from Step 1 is simulated with a lower temperature, such that its chemical composition is readjusted to its new temperature.
- Step 3 simulates the reinjection of heat-depleted and oxidized water into the reservoir. The simulation considers the mixing of this water with the native reservoir fluids (water composition: Table 1—injection well, gas composition Table 2—injection well), with a dominance of the injected fluid. In this step, precipitation of the supersaturated minerals occurs until an equilibrium is reached (i.e., until the saturation index, of calcite and iron(III)Hydroxide is SI = 0).

In the last step, PHREEQC calculates the mass (i.e., the moles) of the two precipitating minerals, which generate the scaling at the bottom and in the screened sections of the injection well (i.e., the chemical clogging). Each step described above is modelled under equilibrium conditions. To corroborate that this assumption is valid, and no step is rate limited, an analysis comparing the results from modelling the system under equilibrium and kinetic conditions was conducted (Appendix 1).

The molar amount of clogging minerals formed in one liter of solution in Step 3 was then transformed into mass and then into a volume. The specific weights of each mineral were: 3.4 g/cm^3 for calcite and and 2.71 g/cm^3 for iron(III)Hydroxide:. The resulting volume was assumed to occupy the existing porosity of the gravel pack, thus causing a decrease in its permeability. The relationship between porosity and permeability was modelled using the Kozeny–Carman Eq. (1) (Carman 1937; Xu and Yu 2008):

$$K = \phi \frac{\epsilon^3 D^2}{180(1-\epsilon)^2} \tag{1}$$

where K = permeability [m^2]; Φ = sphericity, ϵ = porosity, D= average diameter of the sand grains [m].

We set sphericity was $\Phi = 1$ since the gravel pack can be considered as spherical particles, and $D = 1.5 \times 10^{-3}$ m corresponding to the average diameter of the gravel pack.

The second aim of the PHREEQC model presented in this work is the simulation of the chemical soft stimulation performed in 2021 on the chemical precipitation. We modified the model presented above to reproduce a step-by-step addition of hydrochloric acid (HCl) into the reservoir, by adding it to the reservoir water and the formerly precipitated minerals predicted by the model or found in the bailer sample. Different scenarios

("cases") are created to evaluate the implication of different dosage on the unclogging capacity of HCl, depending on specific geochemical conditions, such as the expected clogging mineral mass.

Results

On site investigations

Properties of the bailer-collected sample: mineralogical, chemical, microbial composition

The sample from the well bottom sediments had black, graphite-grey colour and intensive smell of hydrocarbon. The material was oily, sticky, and contained only small amounts of sand particles but mainly clays (Fig. 3A). Particles extracted from the bailer-collected sample were strongly magnetic (Fig. 3B).

X-ray Fluorescence analysis of the bailer-collected sample showed the predominance of SiO_2 (43.8 m/m%) and Fe_2O_3 (27.9 m/m%) followed by Al_2O_3 (11.6 m/m%), MgO (3.31 m/m%), K_2O (2.31 m/m%), Na_2O (1.69 m/m%), TiO_2 (0.68 m/m%), MnO 0.3 (m/m%), S (0.27 m/m%), P_2O_5(0.1 m/m%), while the Loss of ignition (LOI) was 7.5 m/m%.

Primary mineral phases of the sample resulting from the X-ray Powder Diffraction (XRD) analyses were clastic sediments, i.e., quartz, clay minerals feldspars and carbonates (Table 3). Main clay minerals were illite, illite–smectite (i/sm 11A: a disordered mix-layer of illite–smectite clay mineral phase with low swelling capacity) and subordinately kaolinite and chlorite. The XRD pattern was interpreted using Rietveld refinement method to define the quantitative mineral composition. Calcite and dolomite accounted for 5% of the total bailer-collected sample material, while iron minerals (hematite, magnetite) presented 12% of the material. The amount of magnetite was remarkably high, being consistent with the Fe_2O_3 content measured by XRF and the very low sulphur content. The average crystal size of the magnetite was very fine, 21 ± 5 nm.

The share of mineral phases with volatile components was low, which suggests that the predominant part of the LOI was from the decomposition of organic matter. Treated with H_2O_2, the sludge showed intensive oxidation (practically boiling) and the colour changed to light brown.

Fig. 3 Material of the bailer-collected sample (**A** left) and material at the downhole equipment (**B** right)

Table 3 Mineral composition of the bailer sample (m/m%)

Mineral phase	Ratio (m/m%)
Quartz	20.4
Magnetite	10.7
Illite	10.1
Muscovite	8.3
Illite–smectite	7.2
Kaolinite	2.3
Chlorite	2.1
Calcite	3.9
Dolomite	1.2
Hematite	1
Albite	3.8
Microcline	0.6
Halite	1.1
Amorphous	27.4
Total	100

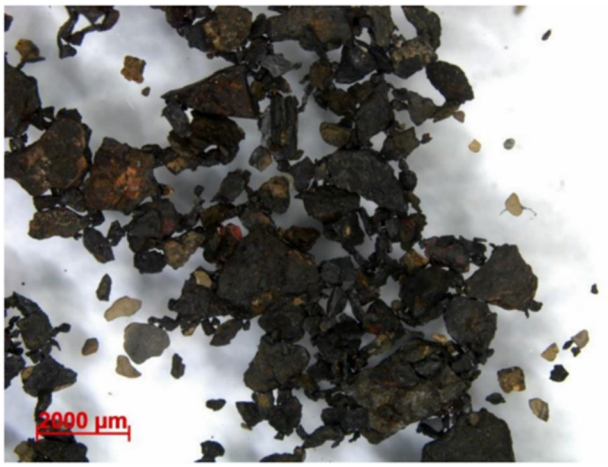

Fig. 4 The magnetic fraction of the bailer sampled material under stereo microscope

The quartz grains comprised approximately 15–20% of the coarse-grained washed subsample, clay rich concretions comprised about 40%, while the magnetic grains formed another ca. 40% of the sample. The surface of the magnetic grains was dull and usually black; some grains had reddish or reddish-brown discoloration on the surface (Fig. 4). Grains stuck to each other due to magnetic attraction. These grains were more solid and resistant to pressure compared to the clay concretions. The maximum observed grain size reached 1.6 mm.

According to the microbial analysis, *Pseudomonas genus* was the most abundant bacteria, being 64% of all the detected microbes (Fig. 5). Additional 7% came from *Pseudomonadales* order while the *Terrabacteria* group formed a rest of 12% among others with *Actinobacteria* and *Firmicutes* phyla.

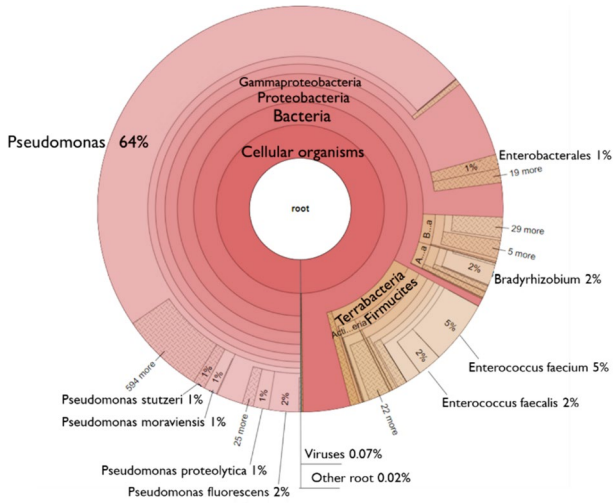

Fig. 5 Microbial composition of the bailer sampled material

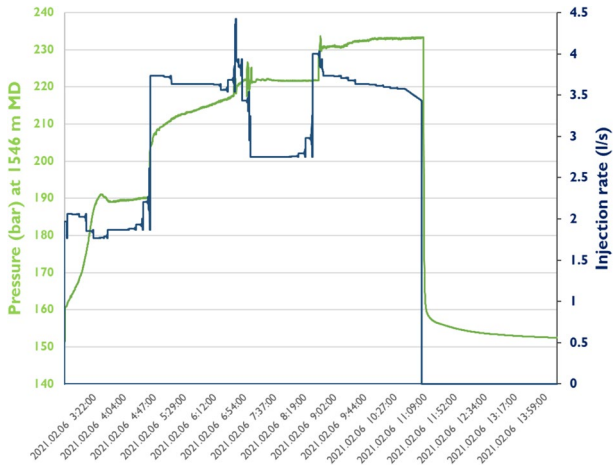

Fig. 6 Downhole data (flow rate and pressure at 1546 m MD) during the step rate injection test

Table 4 Results of the first step rate test: duration, pressure, flow rate and the calculated injectivity index

Duration (min)	Pressure (bar)	Flow rate (l/s)	Flow rate incl. 95% pump efficiency (l/s)	Injectivity index (l/(s·bar))
120	36.4	1.87	1.77	0.049
220	65.2	3.64	3.46	0.053
242	73.4	4.42	4.2	0.057
350	68.9	2.75	2.61	0.038
480	82.1	3.6	3.42	0.042

Results of the injection test

Step rate injection test Results of the downhole measurements recorded during the step rate injection test are plotted in Fig. 6, while the measured surface values (pressure, flow rate) are summarized in Table 4. The corresponding calculated injectivity index (II) was in the range of 0.038–0.057 l/(s*bar), which fit to the values calculated with the downhole measurements (Fig. 6). During the third step, the pumping rate had to be reduced since wellhead pressure exceeded the previously defined maximum value of 60 bars.

The results revealed a permeability thickness (k*h) of 1.5 Dm with a corresponding transmissivity of 1.709×10^{-5} m^2/s. By considering a pay zone of 75.55 m an average formation permeability of 19.85 mD (1.96×10^{-14} m^2) can be assumed. Using the active reservoir length (43.3 m) permeability is 34.64 mD (3.42×10^{-14} m^2). Since the well was completed in a multilayer setting, each layer might be associated with a slightly different permeability.

Furthermore, the curve analyses of the step rate injection test revealed a positive skin of 18.8 indicating a near well bore damage. The skin related pressure drop for the conducted test is about 59.9 bar.

Constant cold water injection The long-term injection test was scheduled as a constant flow injection test. The test duration was approximately 32 h followed by a shut-in of 24 h. In the same way as for the step rate test flow rates and downhole memory tool pressure and temperature at 1546 m MD depth were applied for well test analysis. An estimation of the injectivity index was not reliable for the test as a leakage of the packer occurred.

A permeability thickness of 2.6 Dm with a corresponding transmissivity of 2.96×10^{-5} m^2/s was calculated which equals k = 34.44 mD (3.40×10^{-14} m^2) considering a h = 75.55 m reservoir length or k = 60 mD (5.93×10^{-14} m^2) considering an active length of h = 43.3 m. Furthermore, the type curve analysis shows a damage in the near well bore area, which is associated with a skin of 22.6, similar to the result of the step rate test. A reduction of reservoir quality in the far field—in the range of 68 m—can be interpreted by an increase in the derivative curve at late time.

Second injection test The last injection test was conducted as a second long-term cold-water stimulation treatment. After a few minutes of injection, a leakage of the packer was identified again. That is why it was decided to run the test without a packer. Therefore, the maximum injection pressure was limited to 40 bar. Thus, the test can be described as a constant head test rather than as a classical injection test. An injectivity index II of 0.02 l/(s·bar) was calculated for the final flow period. This is much lower than for the previous step rate test.

The analysis of the reservoir parameters was performed for the shut-in period of the first step of the second injection test. The determined permeability-thickness of 1.7 Dm (and $T = 1.935 \times 10^{-5}$ m^2/s) is comparable to the results of the previous test. The corresponding average permeability is about k = 22.5 mD (2.22×10^{-14} m^2) (where h = 75.55m) or k = 39.26 mD (3.87×10^{-14} m^2) (where h = 43.3). The overall results from the type curve analysis show a skin of 19.8, which is similar to the previous tests.

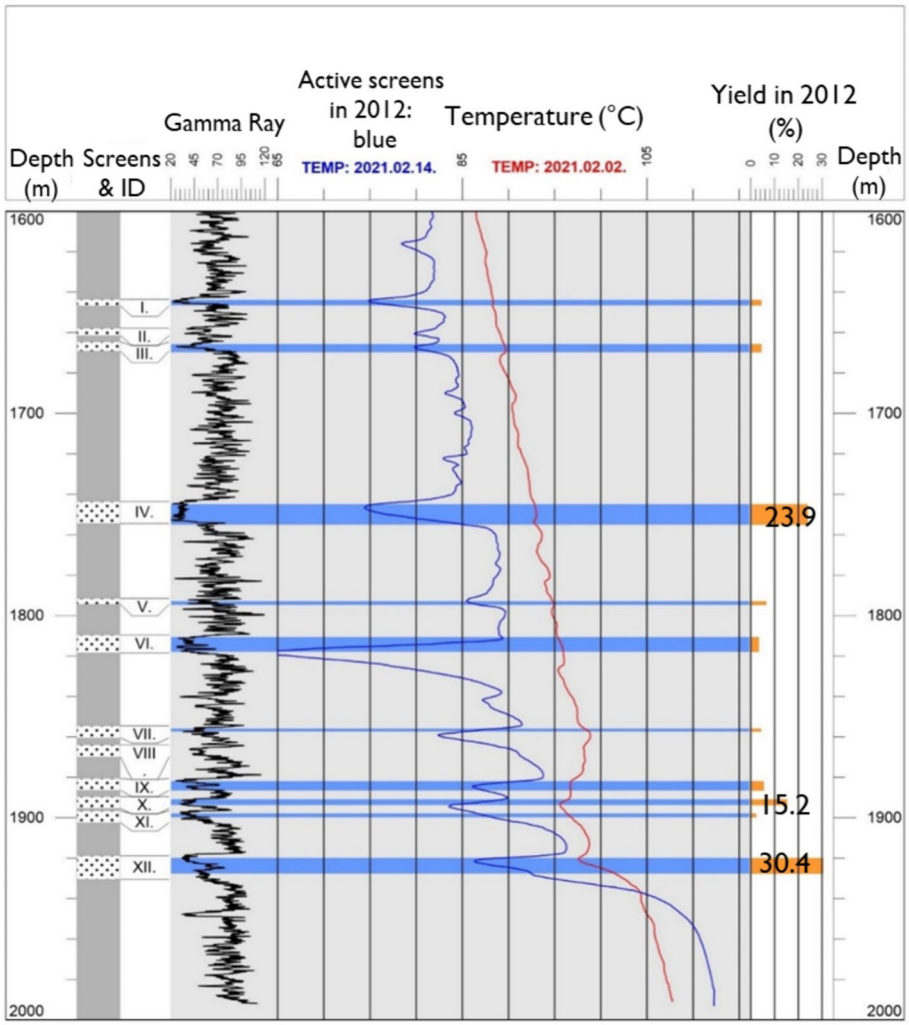

Fig. 7 Position of the screens, gamma ray, temperature logs before (red) and after (blue) cold water injection, yields based on flow meter data from 2012 and 2021

Results from well logging—characterizing the reservoir and the injector

The differential temperature profile in 2021 was used to determine screen activity. During the hydraulic injection test in February (described above), a total volume of 88 m^3 brine and 6 m^3 fresh water was injected. Temperature logs were run prior to starting operations and after injecting inhibited water at winter surface temperature (~5 °C) on location. The temperature decrease was averaged across the screens and divided by the average of the baseline temperature profile before injection. A comparison of these results with data from flow meter logs is shown in (Fig. 7) with temperature curves before (red) and after (blue) injection. The logged sections and running speeds were kept constant to compare final results on the same base line. By analysing the temperature logs run after the injection it is possible to identify inflow zones qualitatively, which are indicated by a negative temperature anomaly. It can be assumed that the higher the temperature change, the more fluid could be injected into this interval and that the zone is open to water injection. According to the derived log, the largest operating screen

interval is in 1743.6–1754.5 m, while same tendency can be observed in the other open intervals: e.g., in 1809.6–1815.6 m, 1918.8–1930.4 m.

Additionally, temperature logs helped to exclude any potential casing damage. This was supported by the cementing and caliper logs analysed by Brehme et al. (2024): the integrity of the well is qualitatively evaluated and assumed that no leaking zones or perforated sections are identified in the casing strings or overlaps.

The obtained gamma ray log (from 2021) was compared with the one from 2012 to observe any potential changes which could indicate trapping of fine sediments or outwashed grains. The two logs (Fig. 8) show clear similarities without significant deviations.

Screened section evaluation was carried out based on Dual Space Neutron log: near (Fig. 9B) and far (Fig. 9C) neutron counts combined with Gamma Ray and Casing Collar Locator logs (A). Near/far ratio (Fig. 9D) show higher and lower qualitative density contributions proportional to the ratio, hence the count rate will be low in higher porosity sections.

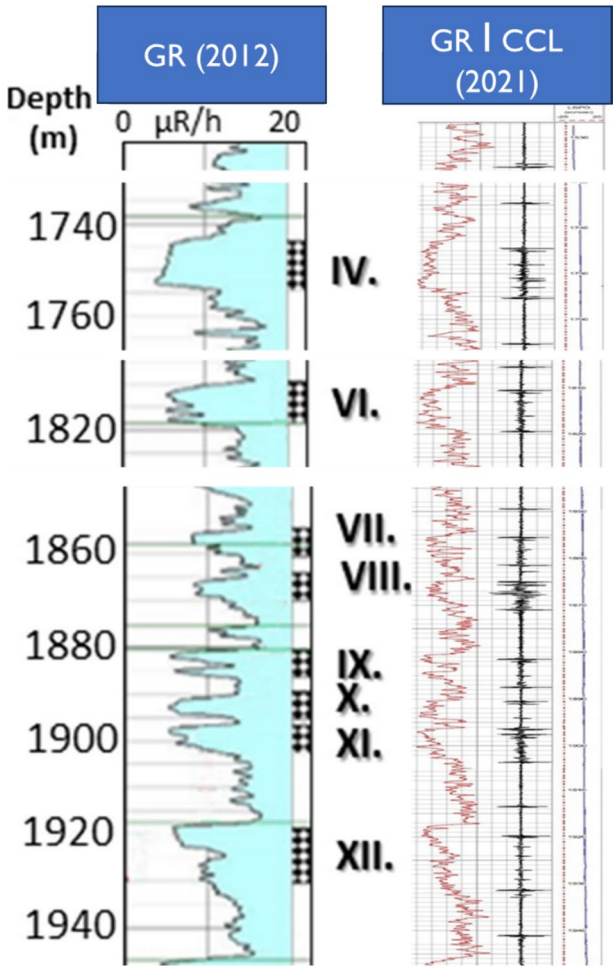

Fig. 8 Comparison of gamma ray logs with the screen number IV and VI-XII (Left: GR log from 2012, right: GR and CCL log from 2021 February)

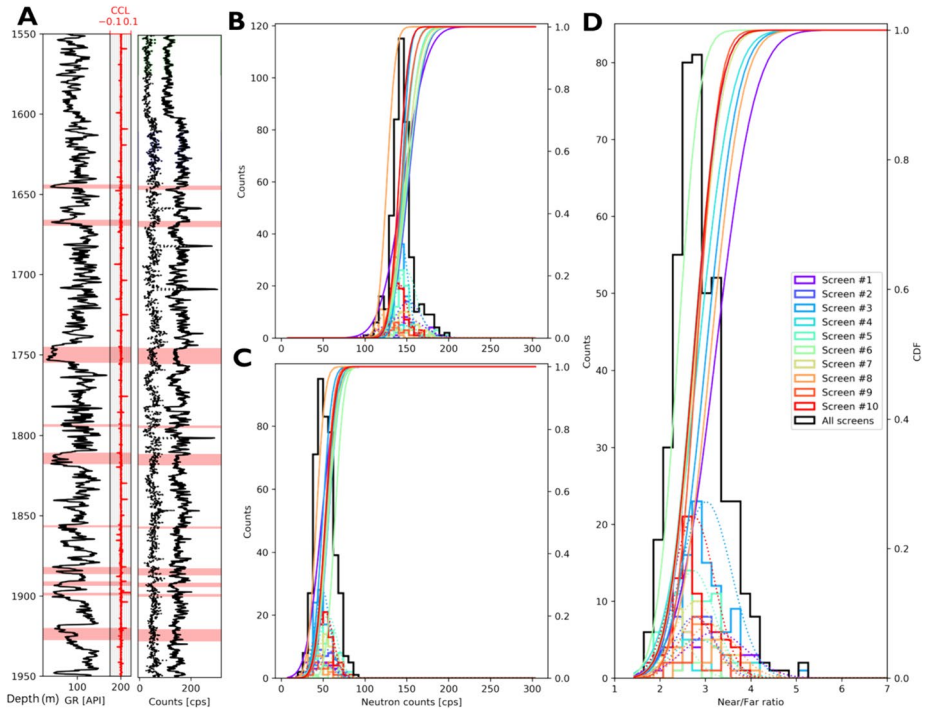

Fig. 9 Screened sections evaluation based on neutron counts: Gamma Ray (GR), CCL (Casing Collar Locator), and Neutron logs (**A**); For all screens (black) and broken down into the 10 individual screened intervals, Near (**B**), Far (**C**) and near/far ratio (**D**) show higher and lower qualitative density contributions proportional to the ratio

Table 5 Filter screens dimensions used in the ranking based on available logging data and the estimated volume of chemicals to treat the reservoir

Screen	Top	Base	Volume, (m^3)
1	1643.9	1646.5	2.51
2	1665.8	1669.7	2.51
3	1745	1755	4.57
4	1793	1794.7	2.61
5	1810.7	1817.9	4.10
6	1856	1857.3	2.60
7	1882	1886.5	4.55
8	1891	1893.7	4.65
9	1898	1899.8	2.54
10	1920	1927.6	4.63

Using the near and far neutron count ratio (Fig. 9D)—as an indicator of density and porosity variation—the average temperature decrease—(calculated from the differential temperature profile, Fig. 7) as an indicator of the screen activity, and the filter screen width (dz)—as indicator of gravel pack volume—proposal for chemical injection volumes to treat the reservoir was derived: Ten sections with a total length of 43.3 m were chosen to be stimulated as shown in Table 5.

Table 6 Details of the forming scales: volumes formed per 1 L water and volumes formed per day using the average flow rate of 350 L/min

Mineral	Amount of scale (mol/L_w)	Molar weight (g/mol)	Density (g/cm^3)	Volume formed (m^3/L_w)	Volume formed (m^3/day)
Calcite–$CaCO_3$	4.44×10^{-5}	68	3.4	1.13×10^{-9}	5.68×10^{-4}
Iron (III) hydroxide–$Fe(OH)_3$(a)	2.16×10^{-5}	106	2.71	6.47×10^{-10}	3.4×10^{-4}

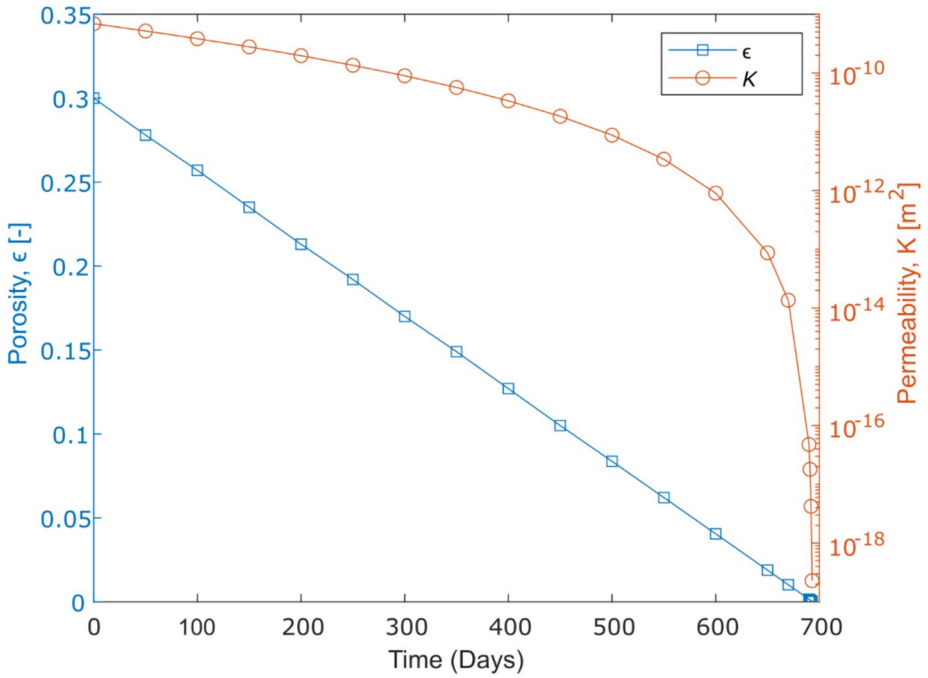

Fig. 10 Calculated reduction in porosity (ϵ) and permeability (K) due to progressive clogging driven by the precipitation of $Fe(OH)_3$(a) and calcite

Hydrogeochemical modelling

Normal operation

Analysis of the amount of scale formed per day is summarized in Table 6. A flow rate of 350 L/min was used in the calculation as an average planned flow rate of the Mezőberény system. Results suggest that within one day 5.68×10^{-4} m^3 calcite and 3.4×10^{-4} m^3 iron(III) hydroxide is formed.

The volume of the ring space was calculated as $V = 5.16$ m^3, by considering the screened interval equal to 75.5 m and a thickness of the gravel pack equal to 0.106 m (considering an inner diameter of 114 mm and an outer diameter of 220 mm). Assuming an average initial porosity for gravel equal to $\epsilon = 30\%$, the pore volume of the gravel pack was calculated as 1.55 m^3. By cumulating the amount of the forming scale (Table 6: calcite: 5.68×10^{-4} m^3/day + iron(III)hydroxide: 3.4×10^{-4} m^3/day), porosity degradation was calculated and plotted in Fig. 10.

Based on the PHREEQC results, a theoretical complete plugging of the pore volume (i.e., $\epsilon = 0$) would be attained in about 2 years. A 50% reduction in porosity would take

place in about one year and would cause a permeability decline of one magnitude based on the Kozeny–Carman equation.

Regarding the sensitivity of the model, the time of clogging is proportional to the initial porosity, i.e., reducing the porosity to half results in a half long complete plugging. The corresponding one magnitude permeability decline also occurs twice as fast. One of the main controlling factors of the hydrogeochemical processes is the air contact: excluding the mixing with the air results in an undersaturation of iron(III) hydroxide, accordingly with the lack of its precipitation the total plugging of the pore space would occur one year later. Reducing the injection temperature from 50 °C to 30 °C results in a slightly higher amount of iron(III) hydroxide but with a half as much calcite, resulting in a slower clogging.

Chemical soft stimulation

To tackle the question of the chemical stimulation from a hydrogeochemical point of view, we simulated the effect of a chemical stimulation. In April 2021, stimulation was carried out using 20% HCl, which equals to 5.5 mol of HCl per liter of solution. Accordingly, 5.5 mol of HCl per liter of reservoir fluid were added in 30 steps combined with dissolved gas and equilibrated with the precipitated minerals.

In the first tested scenario, the initial mass of such minerals was calculated using the previously presented hydrochemical model. We considered calcite as the main clogging mineral (in line with the results of previous XRD analysis), and magnetite as secondary iron-bearing clogging mineral. The basis for the latter choice was the interpretation that the precipitated Iron(III)hydroxides were transformed to magnetite since their precipitation. Since the standard PHREEQC database phreeqc.dat does not include magnetite as a pure phase, the thermodynamics of this mineral were obtained from adapted from the llnl.dat (Lawrence Livermore National Laboratory) database. The molar amount of precipitating minerals formed in one day (Table 6) was cumulated during the one-month operation, and divided by the calculated pore space in the gravel pack. This equalled in 0.211 mol of magnetite and 0.433 mol of calcite per dm^3 of pore volume. The latter was included as input in the second model set-up simulating the reactions of one liter reservoir water and the addition of HCl. In the second tested scenarios ("Case 2"), we studied the behaviour of a system with a higher initial mass of clogging minerals. Specifically, we set initial mass as twice the mineral mass computed in Case 1; this resulted in an initial calcite mass of 0.866 mol and an initial magnetite mass of 0.422 mol.

The results of the simulations are summarized in Fig. 11. For both scenarios, we found a significant drop in the saturation of the clogging minerals. For calcite, only 1 mol of HCl allow removing the entire scaling (Fig. 11a). Full dissolution of magnetite requires the addition of 2.5 mol of HCl (Fig. 11b). The delayed dissolution of magnetite can be explained considering that, when all calcite is dissolved, pH quickly drops to pH = 2, rendering water extremely acidic and aggressive also for magnetite (Fig. 11b). Similar conclusions can be made in case of doubling the amount of precipitated minerals. The higher mineral mass requires a larger amount of 5.2 mol of HCl to completely dissolve calcite and magnetite. Because calcite requires more HCl to be dissolved, pH remains buffered to values close to pH = 4–5 for longer time, keeping magnetite mass constant. When all calcite is dissolved, magnetite starts dissolving at lower pH, as in Case 1.

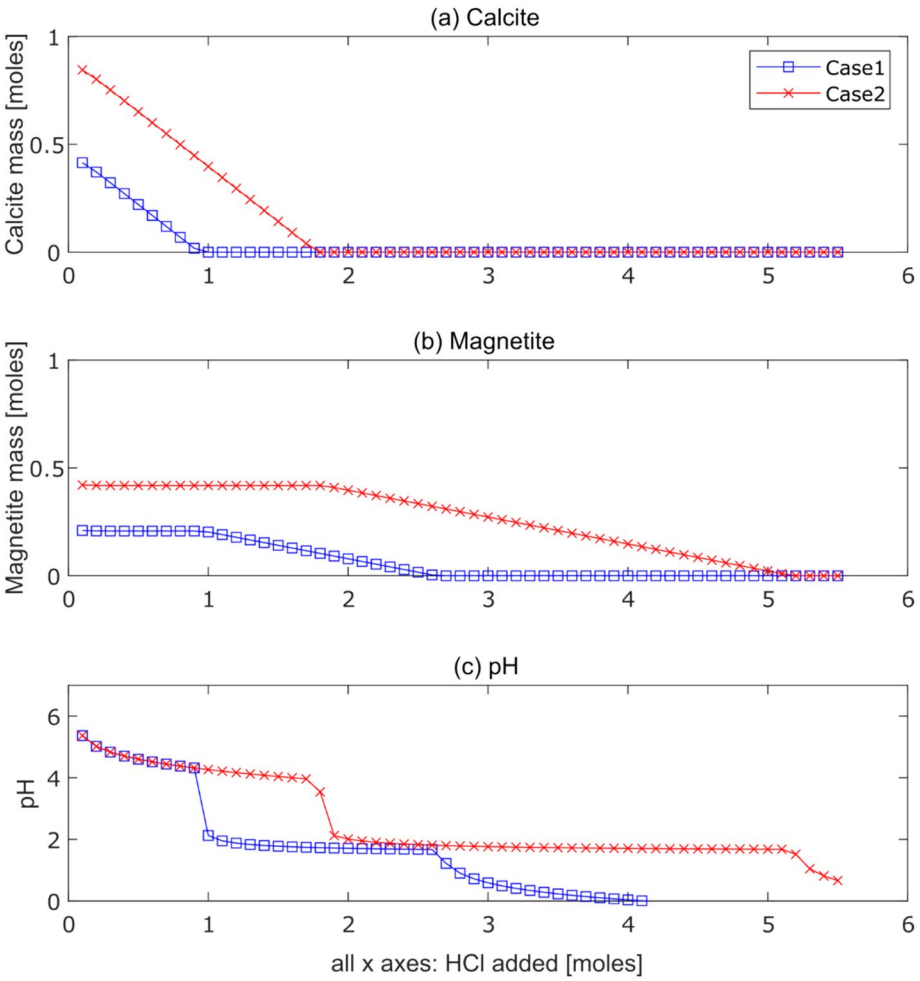

Fig. 11 Change of calcite (**a**) andmagnetite (**b**) mass during the HCl acidization (**c**) reports the pH decrease. All horizontal axes represent the addition of HCl (moles)

Joint interpretation and discussion

In the former studies, the insufficient reservoir transmissivity along with physical, chemical and biological clogging processes were assumed to be responsible for the low injectivity (Brehme et al. 2019b; Markó et al. 2021). To prove the injection problems and to tailor the remediation strategy, reservoir behaviour as well as the occlusion of flow pathways was analysed in detail combining historical data and the new dataset gained during the field campaigns in spring 2021.

Reservoir behaviour

The initial reservoir indicators (sandstone content, permeability) are relatively inferior compared to reference sites and to the proposed literature value, which indicate a low reservoir performance (Willems et al. 2019, 2021; Markó et al. 2021). The low net sandstone content is further narrowed by the limited volumes connecting the production and injection wells which contributes to the low injection rate (Willems et al. 2019; Budai et al. 2024).

The well tests of the on-site campaign confirmed that the injection capacity is low. The permeability thickness (k*h) is in the range of 1.5 Dm to 2.6 Dm and the corresponding permeability ranges between k = 19.85 mD = 1.96 × 10^{-14} m^2 and k = 34.44 mD = 3.40 × 10^{-14} m^2 assuming a pay zone of h = 75.55 m which is the total length of the well screens. For comparison, permeability derived from the pressure build-up test performed after the well completion (2012) was k = 50.4 mD = 5.4 × 10^{-14} m^2 (Markó et al. 2021). Accordingly, a 30–60% permeability decline was observed.

All injection tests showed that the near-wellbore area is associated with a very high skin between 18.8 and 22.6 indicating a massive obstacle for fluid flow. This resulted in a low injectivity index of the well in the range of 0.04–0.06 l/s/bar as calculated from the step rate tests.

Mechanism of clogging processes

In general, the physical, chemical and biological processes causing injection problems can partly be triggered by the injection (Brehme et al. 2018) or caused by the disturbed physico-chemical equilibrium (Szanyi et al. 2014). Regarding the chemical and physical mechanism, clogging is formed either as material attached to surfaces (i.e., scaling or microbial biofilm narrowing the pipelines and wellbore), or as transported materials originated from reservoir particles, precipitated minerals or bioproducts which result in the plugging of surface filters and well screens (Barkman & Davidson 1972; Seibt and Kellner 2003) as experienced in the Mezőberény case.

A risk of pore blocking in certain reservoir sections by fines migration was understood from former data (Markó et al. 2021). Especially, the less cemented reservoir sections were assumed to pose a risk of releasing fines during production and injection in long-term operation. However, comparing the gamma ray logs from 2012 and 2021, they show clear similarities (Fig. 8). There are no significant differences in the grain sizes of the single screens, therefore a change in the grain size in these segments (due to outwashing or trapping of fines at the screens) cannot be confirmed. At the same time, the bailer sample taken in February 2021 showed relatively high clay content.

Results of our hydrogeochemical model suggest a relatively high amount (6.66 × 10^{-5} mol/L) of scales (calcite, iron(III)hydroxide) to precipitate at the Mezőberény site. Carbonates and iron oxides-hydroxides have been detected in surface filter samples in 2017, as well as in the bailer sample taken during the on-site campaign, shown by the XRD analysis. Main source of the carbonate can be the calcite cement of the sandstone rock dissolving in the thermal water (Willems et al. 2021; Koroncz et al. 2022). Since no larger particles of the materials were found in the sample, larger accumulations of precipitated minerals are not expected but rather smaller particles that can block pore space in the reservoir rock or in the gravel pack.

Based on our calculation the precipitation of iron and carbonate minerals would be responsible for the porosity and permeability degradation on a long-term operation by decreasing the permeability with one magnitude over approximately 2 years (Fig. 10). However, the plugging of the screens was experienced within a short period, i.e., one month, therefore other processes probably account for the clogging issue more significantly.

The two microbial analyses from the filter residual (2017–(Markó et al. 2021)) and the bailer sample both from the injection site (2021) clearly differ: In the filter residual (2017) sulphate reducing bacteria and methanogenic archaea were detected and assumed to be responsible for biofilm formation. Although they were partly present in the bailer sample (2021), their amount is negligible. The most significant similarity is the presence of *Pseudomonas* which was found both in the thermal water from the production well (6%—Markó et al. 2021) and in the bailer sample from the injection well. Its dominance in the bailer sample is high with over 75% of the reads. As *Pseudomonas* is an aerobic, polycyclic aromatic hydrocarbon (PAH) and phenol degrading microorganism, its presence is linked to large amounts of phenol (2012: 5540 µg/L) and significant amount of PAH in the fluid sample of the injector. The high organic content of the bailer sample indicated by the decomposed loss of ignition also proves the favourable conditions for the bacteria. The fluid air contact due to the structure of the surface facilities also triggers the growth of aerobic bacteria.

The nano-particle size (d: 21 ± 5 nm) of the magnetite indicates that the X-ray amorphous material is mainly composed of reduced Fe-oxide(s). Precipitation of magnetite and siderite is expected at reducing, alkaline environments which might take place in the bottom of the reinjection well under presence of bacterial activity. The latter also shows the activity of Fe(III)-reducing bacteria in the sludge. Activity of Fe(III)-reducing bacteria, such as *Geobacter sulfurreducens* or *Shewanella oneidensis* combines the oxidation of organic compounds or hydrogen with reduction of minerals with short-range order (e.g., ferrihydrite), leading to release of Fe^{2+}_{aq} and precipitation of siderite ($FeCO_3$) and magnetite (Fe_3O_4) (Byrne et al. 2011). However, their share in the microbial sample is minimal (0.00008%). Extraction of magnetic material from the bailer sample can be also a sign of corrosion of the pipes or well completion as well, although logging did show a good well integrity. Still, smaller corrosion particles could also contribute to the high skin.

Based on the presence of the Iron(III)-reducing bacteria, it can be assumed that the chemically formed Iron(III) hydroxides—indicated by the hydrochemical models and detected in the filter residuals in 2017—were microbially reduced to magnetite being present in the well-bottom sediments. Accordingly, the microbial activity in the reducing environment is the reason why the nano grain size magnetite and not Iron(III) hydroxide were detected by the XRD analysis. This is a good example of the interaction of the two (chemical and biological) mechanisms highlighted by previous studies (Sand 2003; Brehme et al. 2018). Additional interactions can be expected in the biofilm formation process: extracellular polymeric substances—which embed the microbial cells forming the biofilms—can also contain metal ions (Sand 2003), while forming scale particles can be jointly aggregated with the biofilm material.

Impact of the chemical stimulation

In the framework of Enhanced Geothermal Systems, hydraulic, chemical and thermal stimulation treatments have been applied in the past to enhance reservoir transmissivity with diverse success. The concept of soft stimulation was introduced in the DESTRESS project covering geothermal reservoir stimulation techniques enhancing the reservoir performance while keeping the risk of environmental hazards (including induced

seismicity) low (Huenges et al. 2021). Hydraulic stimulation is the most effective in case of naturally fractured rocks with high shear stress and low permeability, however, the porous reservoir in Mezőberény with a general high permeability as well as the structure of the injection well made it not favourable for high pressure stimulation. Application of chemical stimulation showed higher potential in our case: solving precipitated minerals and soluble minerals of the reservoir rock could open clogged or new flow pathways (Huenges 2011). Acidification of the near-wellbore zone enhanced the transmissivity by reducing the skin from 18–22 to − 0.37 and increased the injectivity from the range of 0.038–0.057 l/s/bar to a range of 0.41–0.75 l/s/bar which means a 4–10 times higher injectivity than at the beginning of the project (Brehme et al. 2024). Accordingly, along with the dissolved mineral precipitation the acidification removed the biological clogging material from the wellbore. Accordingly, flow pathways in the gravel pack and in the near-wellbore reservoir were opened by removing the plugging material from the pore throats and pore space. Based on our understanding this could be feasible both by (i) physical removing the bioproducts; and (ii) by chemically dissolving the scaling that could help mobilizing the mixture of biological and chemical clogging material. A strong pH decline with the addition of HCl from pH 5.37 to 0 was simulated, which resulted in a significant drop in the saturation of the investigated minerals. The amount of the precipitated minerals (Case 1: using the outcome of the normal operation model) is fully dissolved at the addition of 2.5 mol of HCl per liter of water (Fig. 11). In case of doubling, the amount of precipitated minerals (Case 2), total dissolution occurs at the amount of 5.2 mol of HCl. Assuming that Case 1 represents the correct amount of precipitation deposited in the gravel pack, a less concentrated HCl solution (~ 10%) could have dissolved and removed the scaling. However, using the more concentrated (20%) solution has the beneficial effect of dissolving a higher amount of scaling (Case 2) as well as the carbonate minerals of the matrix near the wellbore. Similar or further developed (e.g., reactive transport) hydrochemical models can be useful tools to determine the optimal amount and/or concentration of acid applied during the chemical soft-stimulation.

Suggestions on further development of the site before going into operation

After the successful stimulation, in a long-term operation, clogging processes would still act and should be mitigated by proper measures. High amount of *Pseudomonas* in the production well as well as in the bailer sample and the high amount of organic compound indicate a long-term risk of biofilm formation in the heating system. Mitigation techniques (e.g., constant dosage of biocide) have to be considered for a sustainable run of the plant. Furthermore, constant monitoring of the surface system at strategic locations is necessary. This can cover determining the origin of the particles to effectively avert their entrapment.

Moreover, reconstruction of the surface system is still required. The original system at certain points is open to air inflow (buffer tanks after the production well and before reinjection well). Fluid air contact contributes to clogging processes triggering precipitation and the microbial growth of aerobic bacteria (Markó et al. 2021). Additionally, reducing the mesh size of the filters before the injection to 1 µm would help to filter the potentially forming suspended materials.

A complete remediation requires further analysis to avoid adverse effects resulting in continued injectivity instead of reaching a long-term enhancement. This has been experienced, e.g., in the case of the Klapeida (Lithuania) geothermal site, installed in a siliciclastic reservoir, where artificial treatments led to interaction of the chemical-biological and physical processes: the application of organic based inhibitor presumably triggered microbial activity, while the acidification treatments contributed to additional corrosion (Brehme et al. 2017).

Applicability and limitations

The methodology presented, encompassing the field campaign approach, on-site and laboratory observations, both analytical and theoretical methods, is generally applicable for investigating the causes of low injectivity in sedimentary aquifers: Well tests and well logs contribute to the quantification of the injectivity drop and to understand the behaviour and response of the reservoir. Mineral, chemical, and microbial analysis of well-bottom sediments provides qualitative insights to the nature of clogging materials. Predictions and quantitative assessment are provided by a hydrogeochemical model set-up forecasting the rate of forming of chemical precipitation and its effect on the porosity degradation sor enhancement via the chemical stimulation.

Further step of the research should be an experimental validation of the equilibrium model, which is the main limitation of the current study. Another possible addition is the consideration of the transport effects—which are not taken into account by the presented model—by developing a reactive transport model simulating the near-wellbore zone. Along with the findings of Brehme et al. (2024) this methodology contributes to a successful planning and implementation of soft chemical stimulation in porous reservoirs.

Summary and conclusions

Low injectivity has been experienced in the geothermal site of Mezőberény (SE Hungary). To fully understand the processes taking place in the injection well, borehole tests, logging and sampling were carried out in February 2021, and presented in the current work. A significant damaged zone around the well was discovered, indicated by a skin factor of 18.8–22.6. Permeability was observed to be lower compared to earlier production tests conducted after completion in the range of 19–34 mD.

The reason behind this as highlighted by the novel analysis was the significant fluid flow barrier caused by chemical and biological clogging processes: Analysis of the well-bottom sample revealed high number of *Pseudomonas* bacteria. This group is in its favourable environment due to the high organic and high phenol content of the fluid and its revitalization is triggered by the air contact. Hydrogeochemical modelling suggests precipitation of calcite and iron(III) hydroxides. The chemical products are predicted to be created in small sizes and accumulated in the near-wellbore zone thus contributed to the high skin. Their cumulated amount would cause a significant permeability decline in long-term, but not on a monthly scale. Therefore, it can be assumed that the microbial products have a more significant role in the clogging process. Interaction of microbial and chemical processes is expected in the formation of microbially reduced magnetite. The latter can be part of the highly magnetic portion of the sample along with corrosion products.

Pre-analyses of the previous studies (Brehme et al. 2019b; Markó et al. 2021) and the novel investigations in this current study helped to tailor the soft stimulation to reach an increase in injectivity by 4–10 while mitigating the environmental and operational risks. Chemical stimulation of the near-wellbore zone carried out in 2021 dissolved the precipitation, removed the biological products and decreased the high skin to – 0.37 (Brehme et al. 2024). When modelling the chemical stimulation, the estimated amount of precipitated minerals (Case 1) was dissolved already with 2.5 mol of HCl per liter water (~ 10 m/m%). Therefore, the 20 m/m% of HCl chosen during the field campaign might had beneficial effect dissolving a potential higher amount of scaling (Case 2) and/or the carbonate minerals of the matrix near the wellbore.

This study and the enhanced injectivity established by the stimulation can serve (1) as a first step in restoring the study site—still limited by the low initial reservoir performance; as well as; and (2) a good illustration of a combined investigation using on-site measurements, laboratory analysis with theoretical methods and understanding of the interaction between reservoir scale and clogging processes. A successful restart requires an improved operational strategy to prevent recurrent biological and chemical clogging, along with a professional adaptation of the thermal water circuit above surface infrastructure. This research again indicates that it is crucial to reveal the causes of pore clogging at an early stage to prevent prolonged deterioration of the aquifer.

Appendix 1

See Fig. 12.

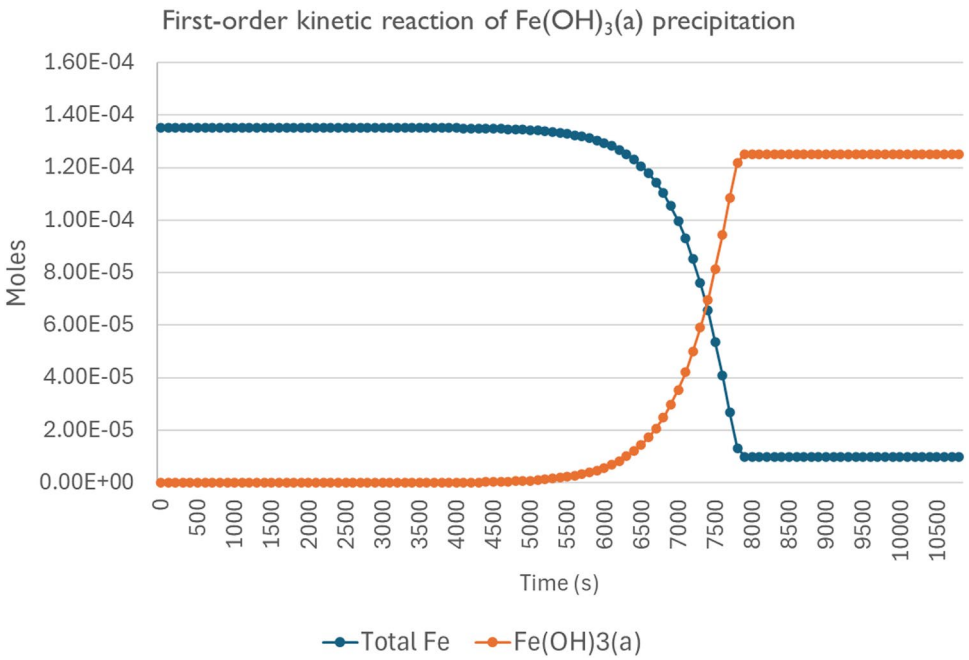

Fig. 12 First order kinetic reaction of $Fe(OH)_3(a)$ precipitation limited by the existing iron in the system. Simulation period: 10,800 s

Geochemical modelling was conducted to investigate the rate of key reactions occurring during the thermal water use. This helped to decide whether an equilibrium model is appropriate for the simulation. The simulation period was selected to be 10,800 s which is equal to the assumed residential time of the geothermal system derived from the extent of the buffer tank (50 m^3) and the average—production and reinjection—flow rate (350 l/min) of the Mezőberény site. For this analysis, phreeqc.dat database was modified by removing Goethite and keeping $Fe(OH)_3(a)$ as the only iron hydroxide to avoid any potential disturbance.

Before that, as a sensitivity analysis we used kinetic models to investigate the speed of the precipitation and dissolution reactions occurring during the thermal water use. Kinetic model shows the moles of Iron (III) Hydroxide scales forming during the operation of the Mezőberény site (Appendix: Fig. 12). Since the reaction finishes within the residential time of 10,800 s (Appendix: Fig. 12), it can be assumed that the equilibrium is reached within this period, which enables the use of equilibrium models in the following.

Appendix 2

See Figs. 13, 14, 15.

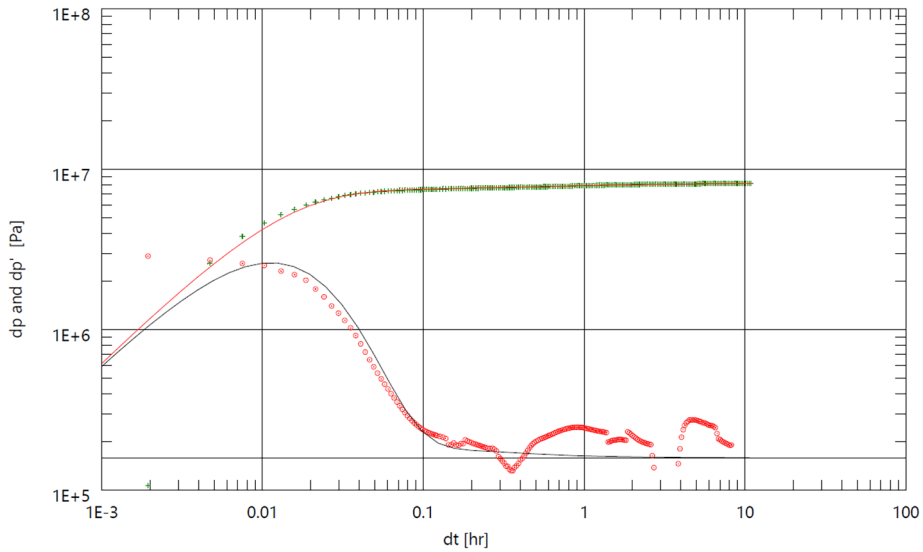

Fig. 13 Well testing in Phase I: Double-log plot of the decline curve including the derivative function for pressure matching

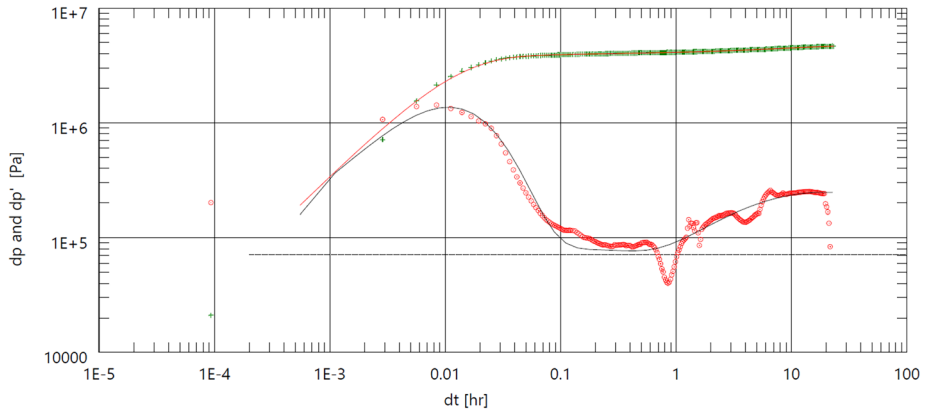

Fig. 14 Constant injection test in Phase II: Double-log plot of the decline curve including the derivative function for pressure matching

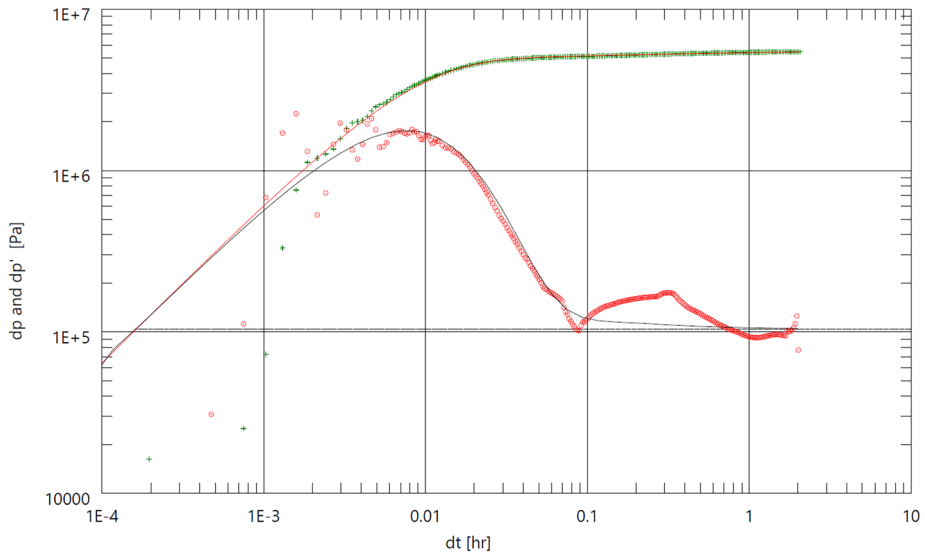

Fig. 15 Step-rate injection test in Phase II: Double-log plot of the decline curve including the derivative function for pressure matching

The evolution of transmissivity (k h) and skin s is calculated from decline pressure curves after each injection stage taking into account the superposition principle and assuming infinite acting radial flow (e.g., Horne, 1995). The calculations are based on the generalized formula for pressure development with stepwise flow rate changes:

$$p(t) = p_0 + \sum_{i=1}^{n} \frac{(q_i - q_{i-1})\mu}{4\pi kh} \left(\mu + ln\left(\frac{\Phi \mu c_t r^2}{4k(t - t_{i-1})} \right) - 2s \right)$$

with p(t), well pressure; p0, initial pressure; h, interval length (height of reservoir); k, rock permeability; qi, flow rate at i-th interval i; μ, dynamic viscosity of fluid; γ, 0.5772 (Euler constant); ti, interval time i; t, total time; Φ, porosity; ct, total compressibility; r, well radius; s, skin.

The transmissivity (k h) is then calculated from the pressure derivative function:

$$\frac{\partial(p_0 - p(t))}{\partial\left(\ln {}^{t}/_{t + t_{inj}}\right)} = \frac{q\mu}{4\pi kh}$$

with q, flow rate; tinj, total injection time; t, duration of fall-off time (shut-in time).

The analysis of the reservoir properties was done by application of type curve analysis using the software package Ecrin Saphir (from Kappa Engineering). The pressure and pressure derivative curves for the model are shown below.

Acknowledgements
Contribution of Santiago Aldaz, Stefan Thiem, Máté Osvald and Wolfgang Weinzierl in designing the field campaigns and interpreting the outcomes is highly acknowledged.

Author contributions
Á.M.: Conceptualization, Data curation, Investigation, Validation, Writing – original draft; M.B.: Conceptualization, Investigation, Supervision, Writing – original draft, Writing – review & editing; Daniele Pedretti: Conceptualization, Formal analysis, Writing – review & editing; Günter Zimmermann: Formal analysis, Investigation, Methodology, Supervision, Writing – review & editing; Ernst Huenges: Conceptualization, Funding acquisition, Resources, Supervision, Writing – review & editing.

Funding
Activities did take place in the frame of the DESTRESS project. The DESTRESS project has received funding from the European Union's Horizon 2020 research and innovation program under grant agreement No 691728. The first author was supported, and the research was financed through the KDP-2021 Cooperative Doctoral Programme of the Ministry of Culture and Innovation of Hungary from the source of the National Research, Development and Innovation Fund, grant number: KDP_2021_ELTE_C1789026. The study was funded by the National Multidisciplinary Laboratory for Climate Change, RRF-2.3.1–21-2022–00014 project. M.B. is supported by the Energi Simulation foundation. The work was partly supported by the Italian Ministry for Universities and Research (MUR) through the project "Dipartimenti di Eccellenza 2023–27".

Availability of data and materials
The data that support the findings of this study are available within the article, microbial dataset is available from the corresponding author, upon request.

Declarations

Ethics approval and consent to participate
Not applicable.

Competing interests
The authors declare no competing interests.

Received: 15 May 2024 Accepted: 15 September 2024
Published online: 22 October 2024

References

Alsemgeest J, Auqué LF, Gimeno MJ. Verification and comparison of two thermodynamic databases through conversion to PHREEQC and multicomponent geothermometrical calculations. Geothermics. 2021;91: 102036. https://doi.org/10.1016/j.geothermics.2020.102036.
Axelsson G. Role and management of geothermal reinjection. Short course on geothermal development and geothermal well. 2012.
Barkman JH, Davidson DH. Measuring water quality and predicting well impairment. J Pet Technol. 1972;24(07):865–73.
Békési E, Fokker PA, Candela T, Szanyi J, Van Wees JD. Ground motions induced by pore pressure changes at the Szentes geothermal area. SE Hung Geotherm Energy. 2022;10(1):3. https://doi.org/10.1186/s40517-022-00214-6.
Bobok E, Tóth AN. Geothermal energy production and its environmental impact in Hungary. In: International Geothermal Conference. Reykjavík; 2003.
Brehme M, Regenspurg S, Leary P, Bulut F, Milsch H, Petrauskas S, Valickas R, Blöcher G. Injection-triggered occlusion of flow pathways in geothermal operations. Geofluids. 2018;2018(1):4694829. https://doi.org/10.1155/2018/4694829.

Brehme M, Nowak K, Banks DP, Valickas R, Bauer K, Burnside N, Boyce A. A review of the hydrochemistry of a deep sedimentary aquifer and its consequences for geothermal operation: Klaipeda, Lithuania. Geofluids. 2019a;2019(1):4363592. https://doi.org/10.1155/2019/4363592.

Brehme M, Marko A, Nowak K, Istvan S, Blöcher G, Huenges E. Injection-triggered occlusion of flow pathways and its remediation in Mezőberény-Hungary. In: European Geothermal Congress. 2019b.

Brehme M, Markó Á, Osvald M, Zimmermann G, Weinzierl W, Aldaz S, Thiem S, Huenges E. Demonstration of a successful soft chemical stimulation in a geothermal sandstone reservoir in Mezőberény (Hungary). Geothermics. 2024;120:102980. https://doi.org/10.1016/j.geothermics.2024.102980.

Brehme M, Blöcher G, Regenspurg S, Milsch H, Petrauskas S, Valickas R, Wolfgramm M, Huenges E. Approach to develop a soft stimulation concept to overcome formation damage—a case study at Klaipeda, Lithuania. In: Proceedings of the 42nd Workshop on Geothermal Reservoir Engineering. 2017.

Brehme M, Nowak K, Abel M, Siklosi I, Willems C, Huenges E. Injection triggered occlusion of flow pathways in a sedimentary aquifer in Hungary. In: Proceedings world geothermal congress 2020+1 Reykjavik, Iceland, April–October, p 5. 2021. https://pangea.stanford.edu/ERE/db/WGC/papers/WGC/2020/23011.pdf. Accessed 29 July 2021

Budai S, Willems CJ, Colombera L, Westaway R. Influence of sedimentary architecture on static connectivity and geothermal doublet performance (Mezőberény, SE Hungary). Mar Pet Geol. 2024. https://doi.org/10.1016/j.marpetgeo.2024.106820.

Burté L, Cravotta CA III, Bethencourt L, Farasin J, Pédrot M, Dufresne A, Gerard MF, Baranger C, Le Borgne T, Aquilina L. Kinetic study on clogging of a geothermal pumping well triggered by mixing-induced biogeochemical reactions. Environ Sci Technol. 2019;53(10):5848–57. https://doi.org/10.1021/acs.est.9b00453.

Byrne JM, Coker VS, Pattrick RA, Van Der Laan G, Arenholz E, Lloyd JR. Control of nanoparticle size, reactivity and magnetic properties during the bioproduction of magnetite by Geobacter sulfurreducens. Nanotechnology. 2011;22(45):455709.

Carman P. Fluid flow through granular beds. Tl Chem Eng Lond. 1937;1937(15):150–66.

Cosmo RP, Pereira FD, Soares EJ, Ferreira EG. Addressing the root cause of calcite precipitation that leads to energy loss in geothermal systems. Geothermics. 2022;98: 102272. https://doi.org/10.1016/j.fuel.2021.122067.

Czauner B, Mádl-Szőnyi J. The function of faults in hydraulic hydrocarbon entrapment: theoretical considerations and a field study from the Trans-Tisza region, Hungary. AAPG Bull. 2011;95(5):795–811.

Czauner B, Mádl-Szőnyi J. Regional hydraulic behavior of structural zones and sedimentological heterogeneities in an overpressured sedimentary basin. Mar Pet Geol. 2013;48:260–74. https://doi.org/10.1016/j.marpetgeo.2013.08.016.

Czauner B, Simon S, Mádl-Szőnyi J. How to consider groundwater flow systems in the Earth's critical zone?—Demonstration in the Central Pannonian Basin, Hungary. J Hydrol Reg Stud. 2024;53: 101833. https://doi.org/10.1016/j.ejrh.2024.101833.

Dövényi P, Horváth F. A review of temperature, thermal conductivity and heat flow data form the Pannonian Basin. In: Royden LH, Horváth F, editors. The Pannonian basin a study in basin evolution. Tulsa: American Association of Petroleum Geologist memoirs; 1988. p. 195–233.

GeoCom. GeoCom WP5.3. Reinjection to sandstone reservoirs, technology showcase: Reinjection monitoring and modelling (draft version). 2013. https://geothermalcommunities.eu/downloads/14. Accessed 4 Aug 2020.

Gringarten AC. Reservoir lifetime and heat recovery factor in geothermal aquifers used for urban heating. Pure Appl Geophys. 1978;117(1–2):297–308.

Grow JA, Mattick RE, Bérczi-Makk A, Péró C, Hajdú D, Pogácsás G, Várnai P, Varga E. Structure of the Bekes basin inferred from seismic reflection, well and gravity data. In: Basin analysis in petroleum exploration. Dordrecht: Springer; 1994. p. 1–38.

Hörbrand T, Baumann T, Moog HC. Validation of hydrogeochemical databases for problems in deep geothermal energy. Geotherm Energy. 2018;6(1):20. https://doi.org/10.1186/s40517-018-0089-0.

Horváth F, Musitz B, Balázs AV, Uhrin A, Nádor A, Koroknai B, Pap N, Toth T, Wórum G. Evolution of the Pannonian basin and its geothermal resources. Geothermics. 2015;53:328–52. https://doi.org/10.1016/j.geothermics.2014.07.009.

Huenges E. Lectures on enhanced geothermal systems. Reykjavík: United Nations University, Geothermal Training Programme; 2011.

Huenges E, Ellis J, Welter S, Westaway R, Min KB, Genter A, Brehme M, Hofmann H, Meier P, Wassing B, Marti M. Demonstration of soft stimulation treatments in geothermal reservoirs. In: Proceedings of the world geothermal congress. 2020.

Juhász G, Thamó-Bozsó E. Az alföldi pannóniai sl képződmények ásványi összetétele II.-A pannóniai sl homokok és homokkövek ásványi összetétel változásának tendenciái és földtani jelentőségük. Földtani Közlöny. 2006;136(3):431–50.

Kamila Z, Kaya E, Zarrouk SJ. Reinjection in geothermal fields: an updated worldwide review 2020. Geothermics. 2020;89: 101970. https://doi.org/10.1016/j.geothermics.2020.101970.

Kazmierczak J, Marty N, Weibel R, Nielsen LH, Holmslykke HD. The risk of scaling in Danish geothermal plants and its effect on the reservoir properties predicted by hydrogeochemical modelling. Geothermics. 2022;105: 102542. https://doi.org/10.1016/j.geothermics.2022.102542.

Koroncz P, Vizhányó Z, Farkas MP, Kuncz M, Ács P, Kocsis G, Mucsi P, Fedorné Szász A, Fedor F, Kovács J. Experimental rock characterisation of upper pannonian sandstones from Szentes geothermal field, Hungary. Energies. 2022;15(23):9136. https://doi.org/10.3390/en15239136.

Leins A, Bregnard D, Vieth-Hillebrand A, Junier P, Regenspurg S. Dissolved organic compounds in geothermal fluids used for energy production: a review. Geotherm Energy. 2022;10(1):9. https://doi.org/10.1186/s40517-022-00220-8.

Luo W, Kottsova A, Vardon PJ, Dieudonné AC, Brehme M. Mechanisms causing injectivity decline and enhancement in geothermal projects. Renew Sustain Energy Rev. 2023;185: 113623. https://doi.org/10.1016/j.rser.2023.113623.

Mádl-Szőnyi J, Simon S. Involvement of preliminary regional fluid pressure evaluation into the reconnaissance geothermal exploration—example of an overpressured and gravity-driven basin. Geothermics. 2016;60:156–74. https://doi.org/10.1016/j.geothermics.2015.11.001.

Markó Á, Driba D, Zsemle F, Osvald M, Brehme M. Analysis of geothermal reinjection problems with hydrogeochemical modelling. In: Proceedings world geothermal congress. Reykjavik; 2020.
Markó Á, Mádl-Szőnyi J, Brehme M. Injection related issues of a doublet system in a sandstone aquifer—a generalized concept to understand and avoid problem sources in geothermal systems. Geothermics. 2021;97:102234. https://doi.org/10.1016/j.geothermics.2021.102234
Njeru RM, Halisch M, Szanyi J. Micro-scale investigation of the pore network of sandstone in the Pannonian Basin to improve geothermal energy development. Geothermics. 2024;122: 103071. https://doi.org/10.1016/j.geothermics.2024.103071.
Osvald M, Maróti G, Pap B, Szanyi J. Biofilm forming bacteria during thermal water reinjection. Geofluids. 2017;2017(1):9231056. https://doi.org/10.1155/2017/9231056.
Parkhurst DL, Appelo CA. Description of input and examples for PHREEQC version 3: a computer program for speciation, batch-reaction, onedimensional transport, and inverse geochemical calculations. US Geol Surv Tech Methods. 2013;6(A43):497.
Sand W. Microbial life in geothermal waters. Geothermics. 2003;32(4–6):655–67. https://doi.org/10.1016/S0375-6505(03)00058-0.
Seibt P, Kellner T. Practical experience in the reinjection of cooled thermal waters back into sandstone reservoirs. Geothermics. 2003;32(4–6):733–41.
Song W, Liu X, Zheng T, Yang J. A review of recharge and clogging in sandstone aquifer. Geothermics. 2020;87:101857. https://doi.org/10.1016/j.geothermics.2020.101857.
Stefansson VÐ. Geothermal reinjection experience. Geothermics. 1997;26:99–139.
Szanyi J, Kovács B. Utilization of geothermal systems in South-East Hungary. Geothermics. 2010;39(4):357–64. https://doi.org/10.1016/j.geothermics.2010.09.004.
Szanyi J, Medgyes T, Kóbor B, Tari C, Balint A. Experiences with geothermal water injection into porous aquifers. Tech Poszuk Geol. 2014;53:3.
Sztanó O, Szafián P, Magyar I, Horányi A, Bada G, Hughes DW, Hoyer DL, Wallis DL. Aggradation and progradation controlled clinothems and deep-water sand delivery model in the Neogene Lake Pannon, Makó Trough, Pannonian Basin, SE Hungary. Glob Planet Change. 2013;103:149–67. https://doi.org/10.1016/j.gloplacha.2012.05.026.
Sztanó O, Magyar I, Katona L. Lake Pannon and the Balaton in Hungarian: a Pannon-tó és a Balaton. In: Babinszki E, Horváth F (eds.) A Balaton kutatása Lóczy. 2020.
Thamó-Bozsó E, Juhász G, Kovács LÓ. The mineral composition of the Pannonian sl Formations in the Hungarian Plain (I). The characteristics and origins of the Pannonian sl sands and sandstones. Földtani Közlöny. 2006;136(3):407–29.
Tóth J, Almási I. Interpretation of observed fluid potential patterns in a deep sedimentary basin under tectonic compression: Hungarian Great Plain, Pannonian Basin. Geofluids. 2001;1(1):11–36.
Ungemach P. Reinjection of cooled geothermal brines into sandstone reservoirs. Geothermics. 2003;32(4–6):743–61.
VITUKI. Hydrogeological logbook, Mezőberény, K-116. Mezőberény: VITUKI Environmental Protection and Water Management Research Institute; 2012.
Willems CJ, Cheng C, Watson SM, Minto J, Williams A, Walls D, Burnside N, Westaway R. Permeability and mineralogy of the Újfalu formation, Hungary, from production tests and experimental rock characterization: implications for geothermal heat projects. Energies. 2021;14(14):4332. https://doi.org/10.3390/en14144332.
Willems CJ, Westaway R, Burnside NM. Hydraulic connectivity in pannonian sandstones of the Mezőberény geothermal doublet. In: European Geothermal Congress. 2019.
Xu P, Yu B. Developing a new form of permeability and Kozeny-Carman constant for homogeneous porous media by means of fractal geometry. Adv Water Resour. 2008;31(1):74–81. https://doi.org/10.1016/j.advwatres.2007.06.003.
Yanaze T, Yoo S, Marumo K, Ueda A. Prediction of permeability reduction due to silica scale deposition with a geochemical clogging model at Sumikawa geothermal power plant. Geothermics. 2019;79:114–28. https://doi.org/10.1016/j.geothermics.2019.01.002.
Zacherl L, Baumann T. Quantification of the effect of gas–water–equilibria on carbonate precipitation. Geotherm Energy. 2023;11(1):11. https://doi.org/10.1186/s40517-023-00256-4.

Publisher's Note